Materials Research. 2018; 21(5): e20180094
DOI: http://dx.doi.org/10.1590/1980-5373-MR-2018-0094

Enhancing the Supercapacitive and Superparamagnetic Performances of Iron Oxide Nanoparticles through Yttrium Cations Electro-chemical Doping

***Mustafa Aghazadeh*[a]*, *Isa Karimzadeh*[b], *Mohammad Ghannadi Maragheh*[a], *Mohammad Reza Ganjali*[c,d]**

[a]*Materials and Nuclear Research School, Nuclear Science and Technology Research Institute (NSTRI), P.O. Box 14395-834, Tehran, Iran*
[b]*Department of Physics, Faculty of Science, Central Tehran Branch, Islamic Azad University, Tehran, Iran*
[c]*Center of Excellence in Electrochemistry, Faculty of Chemistry, University of Tehran, Tehran, Iran*
[d]*Biosensor Research Center, Endocrinology and Metabolism Molecular-Cellular Sciences Institute, Tehran University of Medical Sciences, Tehran, Iran*

Received: February 07, 2018; Accepted: June 05, 2018

A one-pot electrosynthesis platform is reported for fabrication of Y^{3+} doped iron oxide nanoparticles (Y-IONPs). In this procedure, Y-IONPs are electro-deposited from an additive-free aqueous solution of iron(III) nitrate, iron(II) chloride and yttrium chloride. The analysis data provided by X-ray diffraction (XRD), field emission electron microscopy (FE-SEM) and energy-dispersive X-ray (EDX) confirmed that the deposited Y-IONPs sample is composed of magnetite nanoparticles (size≈20nm) doped with about 10wt% Y^{3+} cations. The performance of the prepared Y-IONPs as supercapacitor electrode material was studied using cyclic voltammetry (CV) and galvanostat charge-discharge (GCD) tests. The obtained electrochemical data showed that Y-IONPs provide SCs as high as 190.3 and 138.9 F g^{-1} at the discharge loads of 0.25 and 1 A g^{-1}, respectively, and capacity retentions of 95.9% and 88.5% after 2000 GCD cycling. Furthermore, the results of vibrating sample magnetometer measurements confirmed better superparamagnetic behavior of Y-IONPs (*Mr*=0.32 emu g^{-1} and H_{Ci}= 6.31 G) as compared with pure IONPs (*Mr*=0.95 emu g^{-1} and H_{Ci}= 14.62 G) resulting from their lower *Mr* and *Hci* values. Based on the obtained results, the developed electro-synthesis method was introduced as a facile procedure for the preparation of high performance metal ion doped magnetite nanoparticles.

Keywords: *Iron oxide, Nanoparticles, Y^{3+} doping, Electrosynthesis, Supercapacitors.*

1. Introduction

Supercapacitors (SCs) have received great attentions among various energy storage devices both in academic and practical applications. They show high power densities and can be fully discharged or charged in seconds, which are suitable for large instantaneous current densities. SCs performance is highly dependent on the specific surface area and conductivity of the electrode materials [1]. The active material of electrode is a determining element of SCs, which dedicate their electrochemical performance. Hence, it is quite understandable that developing efficient and cost-effective electroactive materials be main challenge in the improvement of performance of supercapacitors. Hence, extensive researches have been focused to find proper electrode materials for SCs. Pseudocapacitors mainly store charges from reversible redox reactions and generally composed of transition metal oxides/hydroxides like tin oxide [2], titanium oxide [3], cobalt oxide [4,5], nickel oxide [6-8], vanadium oxide [9], zinc oxide [10], manganese oxides [11-15], cobalt hydroxides [16-20], nickel hydroxides [21-25] and iron oxides [22-32]. This type of SCs could deliver high specific capacitance, but present poor cycle stability. Among metal oxides, magnetite (Fe_3O_4) is the interested candidates as a result of its environmental friendliness, natural abundance, low cost and variable oxidation states [33]. It was found that low electrical conductivity of iron oxide is major obstacle for use as electrode material in ECs [34,35]. For refine this issue, three solutions of novel nano-structures fabricating [36-43], metal ions doping [44], and also combination with conductive carbon-based nanomaterials [45-47] have been established. Reviewing the results of these works indicates that performance of iron oxide electrode is improved due to enhancing its conductivity and redox activity. Notably, metal ion doping strategy has been rarely investigated. In this paper, we report a novel platform for the preparation of metal ion (Y^{3+}) doped iron oxide nanoparticles (Y-IONPs) through cathodic electrodeposition procedure, and also about 15% improvement in the supercapacitive capability of IONPs as a result of Y^{3+} doping. This platform is based on the well-known cathodic electrosynthesis (CE) method. In this method, nanostructured metal oxides/hydroxide could be easily prepared through OH^- electro-generation on the cathode surface [48-50]. However, this method has not been applied for the preparation IONPs until now. It is worth noting that we very recently reported one-pot electrosynthesis

*e-mail: maghazadeh@aeoi.org.ir.

of naked and polymer coated IONPs through cathodic electrosynthesis (CE) method [51-53]. Here, we applied a CE strategy for the synthesis of Y^{3+} doped IONPs. To the best of our knowledge, electrochemical synthesis of metal doped Fe_3O_4 NPs has not been reported until now. The prepared Y-IONPs were characterized by XRD, IR, FE-SEM, VSM, cyclic voltammetry (CV) and galvanostat charge-discharge (GCD) techniques. The results of these analyses confirmed the proper magnetic and charge storage behavior of the prepared Y^{3+}doped iron oxide NPs.

2.Experimental Procedure

2.1 Materials

Ferrous chloride tetrahydrate ($FeCl_2 \cdot 4H_2O$, 99.5%), ferric nitrate nonahydrate ($Fe(NO_3)_3 \cdot 4H_2O$, 99.9%), yttrium chloride ($YCl_3 \cdot 7H_2O$ 99.9%) and polyvinylidene fluoride (PVDF, $(CH_2CF_2)_n$)were purchased from Sigma Aldrich. All materials were used as received, without any purification.

2.2 Electrosynthesis of Y^{3+} doped Fe_3O_4NPs

The cathodic electrosynthesis (CE) platform previously reported for the fabrication of naked and coated magnetite nanoparticles (MNPs) [51,53], was here modified for the electrosynthesis of Y^{3+} doped IONPs. A schematic view of the preparation route is provided in Fig. 1. The electrosynthesis set-up was composed of a (316 L, 5cm×5cm×0.5mm) steel cathode centered between two parallel graphite anodes, as shown in Fig. 1. The electrolyte solution was prepared by mixing 2g iron(III) nitrate, 1g iron(II) chloride and 0.3g yttrium chloride in 1 liter aqueous solution. The electrodeposition runs were conducted on an electrochemical workstation system (Potentiostat/Galvanostat, Model: NCF-PGS 2012, Iran) with applying *dc* current density of $10mAcm^{-2}$. The deposition time and bath temperature were 30 min and 25º C, respectively.

After each deposition run, the cathode was bring out from solution and rinsed several times with deionized H_2O. Then, the deposited black film was scraped form the steel and subjected to separation and purification steps, as noted in Fig. 1;(i) the obtained wet powder was dispersed in deionized water and centrifuged at 6000rpm for 20min to removal of free anions, as indicated in Fig. 1,(ii) the deposit was then separated from water solution by a magnet, dried at 70º C for 1h, and (iii) the resulting black dry powder was named Y-IONPs, and used for further evaluations.

2.3 Characterization analyses

The SEM images of the prepared powder were provided through field-emission scanning electron microscopy (FE-SEM, Mira 3-XMU with accelerating voltage of 100 kV). The crystal structure of the prepared powder was determined by X-ray diffraction (XRD, Phillips PW-1800) using a Co Kα radiation. The magnetic properties of the prepared Y^{3+} doped IONPs were assessed in the range of −20000 to 20000 Oe at room temperature using vibrational sample magnetometer (VSM, model: Lake Shore, USA).

2.4 Electrochemical tests

Cyclic voltammetry (CV), galvanostatic charging/discharging (GCD) and electrochemical impedance spectroscopy (EIS) were used for electrochemical characterization of the prepared samples. These tests were done using an electrochemical station (AUTOLAB®, Eco Chemie, PGSTAT 30)in a three-electrode set up containing a Na_2SO_3 (1 M) aqueous electrolyte. The three-electrode set-up was composed of working electrode (Y^{3+} doped Fe_3O_4 nanoparticles paste electrode), Ag/AgCl

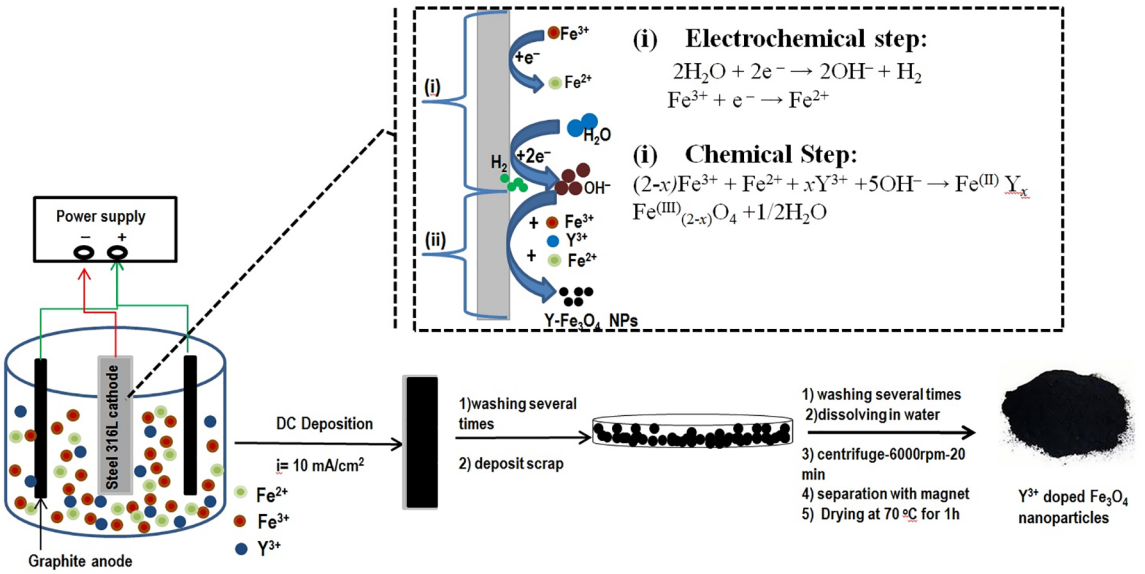

Fig. 1. Schematic graph of the cathodic electrodeposition of Y^{3+} doped IONPs. The inset presents (i) electrochemical and (ii) chemical steps of deposition procedure

reference electrode (saturated with 1 M KCl), and a counter electrode (platinum wire). The working electrode (WE) was fabricated through the well-known paste procedure [34,37]; First, the prepared black Y-IONPs powder was physically mixed with acetylene black (>99.9%) and conducting graphite (with rations of 75:10:10), and the mixture was homogenized properly. Then, 5%wt polyvinylidene fluoride (PVDF) dissolved inN-Methyl-2-pyrrolidone (NMP) was added into the mixture. After partially evaporating the NMP content of the mixture, the resulting paste was pressed at 10 MPa onto Ni foam (surface area of 1cm^2). The resulting electrode was dried for 5 min at about 150 °C in oven. In final, the fabricated electrode was used as working electrode in the electrochemical tests. The mass loading of Y-IONPs powder onto the Ni foam was about 2.5 mg. The CVs of the fabricated working electrode were recorded in a 1M Na_2SO_3 electrolyte in the potential range of -1.0 to+0.1 V vs. Ag/AgCl. The CV profiles were recorded at the potential sweeps of 2, 5, 10, 20, 50 and 100 mV s^{-1}. The GCD curves were recorded at the different current loads of 0.25, 0.5, 1, 2, 3 and 5 A g^{-1} within a potential range of -1.0 to -0.35V vs. Ag/AgCl. The EIS was conducted in the frequency range between 100 KHz and 0.01 Hz with applying 5 mV at open-circuit potential.

3. Results and Discussion

3.1 Structural and morphological characterizations

Fig. 2 shows the XRD patterns of electro-synthesized undoped and Y^{3+} doped Fe_3O_4 powders. All the observed diffraction peaks in the XRD pattern could be readily referred to the pure cubic phase [space group: Fd3m (227)] of Fe_3O_4 with cell constant a = 8.389 Å (JCPDS 01-074-1910).

The purity of the prepared samples was resulted from absence of extra XRD peak in their patterns. Generally, a cubic inverse spinel ferrite structure is reported for crystal structure of Fe_3O_4 , where Fe^{3+} cations are only located in the octahedral sites, but the tetrahedral sites are occupied by both of Fe^{2+} and Fe^{3+} cations [25,29]. It is worth noting that, compared to reflections of undoped sample, small shifts in all reflections of doped sample were observed in Fig 2. These changes are due to the larger ionic radius of Y^{3+} cations toward Fe^{3+} cations (i.e. 92 pm vs. 60pm) [54-57]. From these results, it is stated that Y^{3+} cations are located in some octahedral and/or tetrahedral sites owing to the Fe^{3+} cations in the magnetite crystal structure. Hence, our deposition product has Y^{3+} doped Fe_3O_4 crystal structure. This means that Y^{3+} cations reacted like Fe^{3+} cations during CE process. And the following mechanism could be written for the formation of Y-IONPs [51,52]:

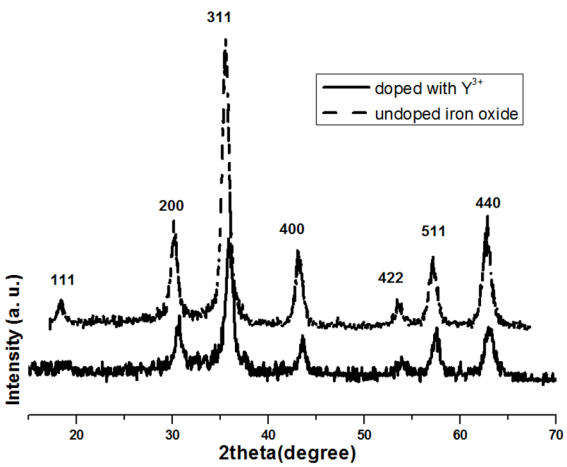

Fig. 2. XRD patterns of undoped and Y^{3+} doped Fe_3O_4 NPs

First, the OH^- ions are generated on the cathode surface through electrochemical step, which shown as step (***i***) in the inset of Fig. 1:

Electrochemical step:

$$2H_2 + 2e^- \rightarrow 2OH^- + H_2 \quad (1)$$

Then, the metal cations i.e. Fe^{2+}, Fe^{3+} and Y^{3+} cations are then chemically reacted with the OH^- generated on the cathode to form iron oxide, which shown as step (***ii***) in the inset of Fig. 1:

Chemical step:

$$Fe^{2+} + (2-x)Fe^{3+} + xY^{3+} + 5OH^- \rightarrow Fe^{(II)}Fe^{(III)}{}_{(1-x)}Y_xO_4 + \frac{1}{2}H_2O \quad (2)$$

In final, the Y^{3+} doped Fe_3O_4 deposited on the cathode and growth during the time of deposition. The average crystallite size (D) of the Y-IONPs was calculated using the Debye-Scherrer equation, $D=0.9\lambda/\beta\cos(\theta)$, where λ is the X-ray wavelength, β is the full width at half maximum of the diffraction line, and θ is the diffraction angle of the XRD pattern. From the diffraction line-width of (311) peak, the average crystallite sizes of the prepared undoped and Y^{3+} doped IONPs were calculated to be 7.2 and 12.1nm.

Figs. 3a-d present FE-SEM images of the electrosynthesized iron oxides. Notably, for better comparison, the FE-SEM images of undoped IONPs have been provided from Refs[52,53]. It is clearly seen that the electrodeposited sample has particle morphology and the particle size in the range of 10-20nm. The elemental analysis of the prepared nanoparticles was provided through energy-dispersive X-ray (EDX), which is presented in Fig. 3e. In this data, it is seen that the electro-deposited Y-IONPs have the Fe, Y and O atoms with the weight percentages of 62.06%wt, 9.78%wt and 28.16%wt, respectively. With considering the fact that Y^{3+}cations plays a same role of Fe^{3+} cations in the CE process, these values are matched with the weight percentages of Fe(72.36%wt) and O (27.64%wt) in the Fe_3O_4 chemical formula. These

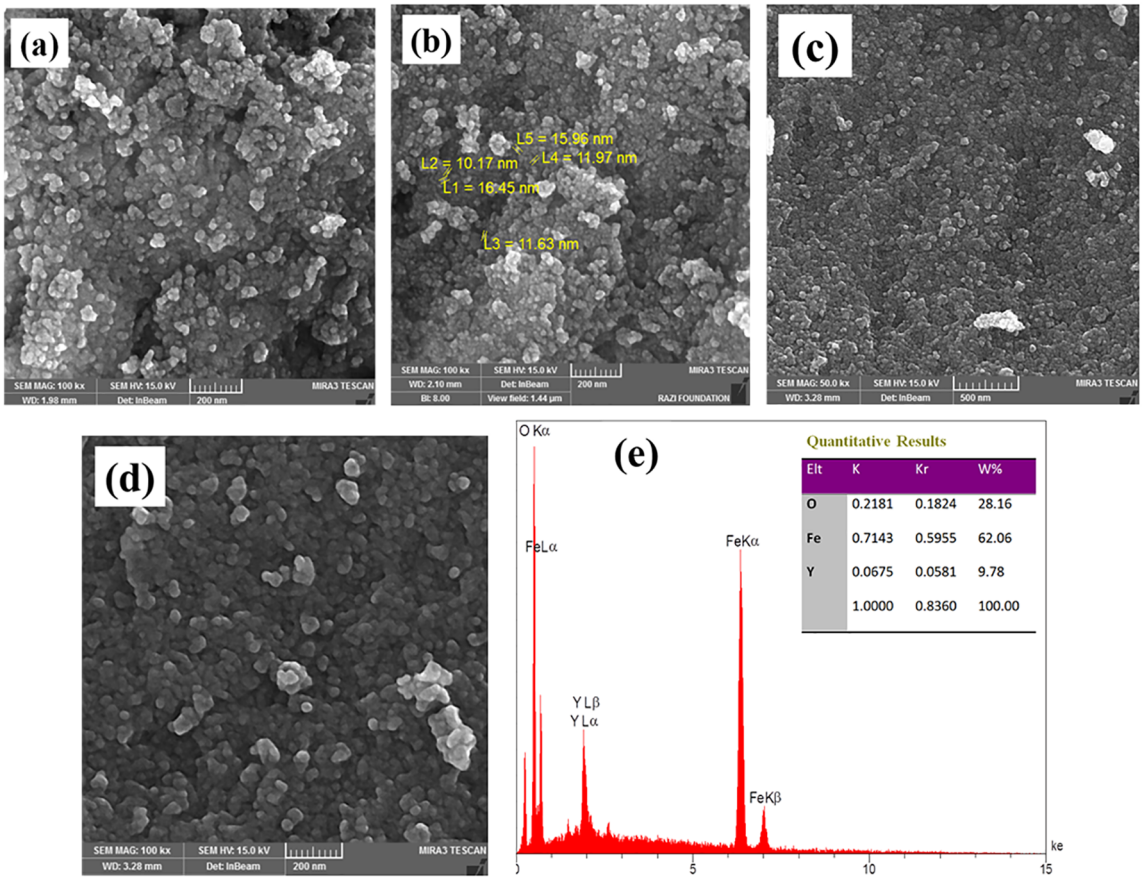

Fig. 3. FE-SEM images of (a,b) undoped and (c,d) Y^{3+} doped iron oxide samples and (e) EDS analysis data

data clearly proved the formation of Fe_3O_4 NPs doped with ~10% Y^{3+} through our developed CE strategy.

The magnetic hysteresis loops for the prepared Sm-IONPs and IONPs (provided from our previous works [52,53]) are shown in Fig. 4. No hysteresis is seen in the VSM profiles and the curves have S like form, as seen in Fig. 4. These observations implicated that the prepared Y-IONPs have superparamagnetic behavior. The magnetic data of the prepared Y-IONPs are listed in Table 1.

For Y-IONPs, the magnetic data i.e. saturation magnetization (*Ms*), remanent magnetization (*Mr*) and coercivity (H_{Ci})are observed to be; *Ms*=43.64 emu g^{-1}, *Mr*=0.32 emu g^{-1} and H_{Ci}= 6.31 G. These data confirmed the superparamagnetic nature of the electrosynthesized Y-IONPs. Also, our Y-IONPs exhibit better superparamagnetic characteristics i.e. higher *Ms* and lower *Mr* and H_{Ci} values as compared with those reported in the literature i.e. Sm^{3+}, Eu^{3+}, Gd^{3+}, Cu^{2+} and Mn^{2+} doped IONPs [54-57]. Furthermore, these magnetic data are comparable with those of undoped IONPs electro-synthesized at a similar electrochemical condition in our previous works. The hysteresis behavior of pure IONPs have been previously studied by the authors, and the reported data are *Ms*=72.96 emu g^{-1}, *Mr*=0.95 emu g^{-1} and H_{Ci}=14.61 G [51,53]. The Y^{3+} doped Fe_3O_4 nanoparticles exhibited low *Ms* compared with undoped Fe_3O_4 nanoparticles, which can be connected to the Y atoms low magnetism compared with Fe ones. However, Y^{3+} doped Fe_3O_4NPs show smaller remanent magnetization and coercivity values as compared with the pure magnetite NPs, which implicated their better superparamagnetic

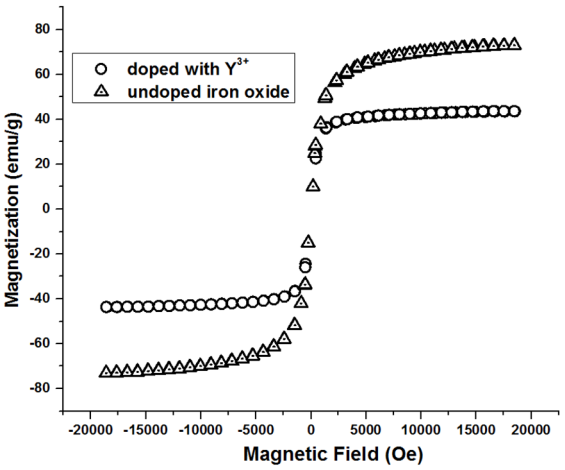

Fig. 4. Hysteresis loops for undoped and Y^{3+} doped iron oxide nanoparticles

Table 1. Magnetic data of the undoped and doped iron oxide nanoparticles

Sample name	Ms (emu/)g	Coercivity (Hci)G	Retentivity Mr (emu/g)	Refs.
Y^{3+}doped IONPs	43.64	6.31	0.32	This work
undoped IONPs	72.96	14.6	0.95	[52]
Sm^{3+}doped IONPs	31.3	85.7	--	[54]
Eu^{3+}doped IONPs	23.6	74.3	--	[55]
Gd^{3+}doped IONPs	32.9	--	--	[56]
Cu^{2+}doped IONPs	53.2	--	--	[57]
Mn^{2+}doped IONPs	61.5	--	--	[57]

nature. Therefore, it is concluded that Y^{3+}doping improves superparamagnetic behavior of magnetite nanoparticles.

3.2 Electrochemical evaluation

3.2.1 Cyclic voltammetry

Cyclic voltammetry was used to evaluate the supercapacitive performance of the working electrode (WE) fabricated from the electrosynthesized Y^{3+} doped IONPs and comparison with undoped ones. Fig. 5a presents the CV curves of the prepared working electrode within the potential range of -1.0 to +0.2V vs. Ag/AgCl with applying the scan rates of 2-100 mV s^{-1}. The shapes of the CV curves clearly reveal the pseudocapacitive characteristics of the Y-IONPs, which is different from the electric double-layer capacitance. In the literature, a combination of both EDLC and pseudocapacitance involving the reduction/oxidation of specifically adsorbed SO_3^{2-} anions on the iron oxide surface has been reported for the capacitance behavior of pure Fe_3O_4 electrode in the Na_2SO_3 solution [39-41], which are seen by small peaks on the CV curve. For Y-IONPs electrode, there are some small peaks i.e. humps on CVs (Fig. 4a) as a result of redox reactions of SO_3^{2-} anions attached onto the surface of Y^{3+} doped Fe_3O_4 nanoparticles [33,35]:

$$2SO_3^{2-} + 3H_2O + 4e^- \longleftrightarrow S_2O_3^{2-} + 6OH^- \quad (3)$$

$$S_2O_3^{2-} + 3H_2O + 8e^- \longleftrightarrow 2S^- + 6OH^- \quad (4)$$

For comparison, a CV data of the working electrode fabricated from the undoped IONPs is also provided, and compared with Y^{3+} doped Fe_3O_4 nanoparticles. Fig. 5b shows the CVs of both undoped and doped IONPs at the scan rate of 5mV/s. It is seen that the Y^{3+} doped IONPs electrode deliver greater anodic and cathodic currents, and hence would have larger SC values.

The SC values of the both working electrodes were calculated from their CV profiles by integrating the area under the current-potential curves using Eq. (5) [18]:

$$C = \frac{Q}{m\Delta(V)}, Q = \int_{V_a}^{V_a} I(V)dV \quad 5$$

where C is the capacitance of prepared Y-IONPs powder (F g^{-1}), Q is the total charge, ΔV is the potential window, *m* is the mass of Y-IONPs powder (g), v is the scan rate (V s^{-1}) and I(V) is the current response during the potential scan. Then, the SCs were plotted vs. scan rate, as shown in Fig. 5c. The calculations revealed that the Y^{3+} doped Fe_3O_4NPs are capable to give SC values as high as 198.7, 174.3, 152.5, 127.8, 99.9, 84.2 and 75.1 F g^{-1} at the scan rates of 2, 5, 10, 20, 50, 75 and 100 mV s^{-1}, respectively. Also, it has been reported that the undoped NPs are enable to deliver SC values of 181,159, 140, 112, 92, 83 and 68 F g-1 at the scan rates of 2, 5,10, 20, 50 and 100 mV s^{-1}, respectively[51-53]. Comparing these SC values revealed that the Y^{3+} doped Fe_3O_4NPs provide up to 10% larger SC values as compared with those of undoped NPs. In other word, it can be said that the supercapacitive performance of iron oxide NPs is increased by Y^{3+}doping into the structure of magnetite. Furthermore, the SC data confirmed the proper charge storage abilities of the electro-synthesized Y^{3+} doped IONPs for use in supercapacitors. The electrochemical behavior of Y^{3+} doped Fe_3O_4 NPs was also investigated by GCD and EIS measurements, which are discussed below.

3.2.2 Charge-discharge tests

Galvanostatic charge-discharge (GCD) profiles of Y^{3+} doped IONPs were recorded at current loads of 0.25, 0.5, 1, 2, 3 and 5A g^{-1} and are given in Fig. 6a.

These GCD profiles are very similar to those reported for iron oxide electrode in Na_2SO_3 electrolyte [28-35], and relative symmetric triangular form at the applied potential range. The form of GCD profiles shows the pseudocapacitance performance of the electrode due to the faradic reactions (Eqs. 3 and 4).The SCs were calculated using Eq. (6)[20], and the data is presented in Fig. 6b:

$$C = \frac{Q}{m \times \Delta V}, Q = I \times \Delta t \quad (6)$$

where C is the capacitance of prepared Y-IONPs powder (F g^{-1}), Q is the total charge, ΔV is the potential window, *m* is the mass of Y-IONPs powder (g), v is the scan rate (V s^{-1}) and I is the applied current load (A) and Δt is the time of a discharge cycle. Notably, some IR drop is also seen in all GCD profiles. The calculations revealed that the Y^{3+} doped IONPs are capable of delivering SC values of 190.3, 159.4, 138.9, 117.5, 96.7, 82, 66.8 and 55.9 F g^{-1} at the discharging

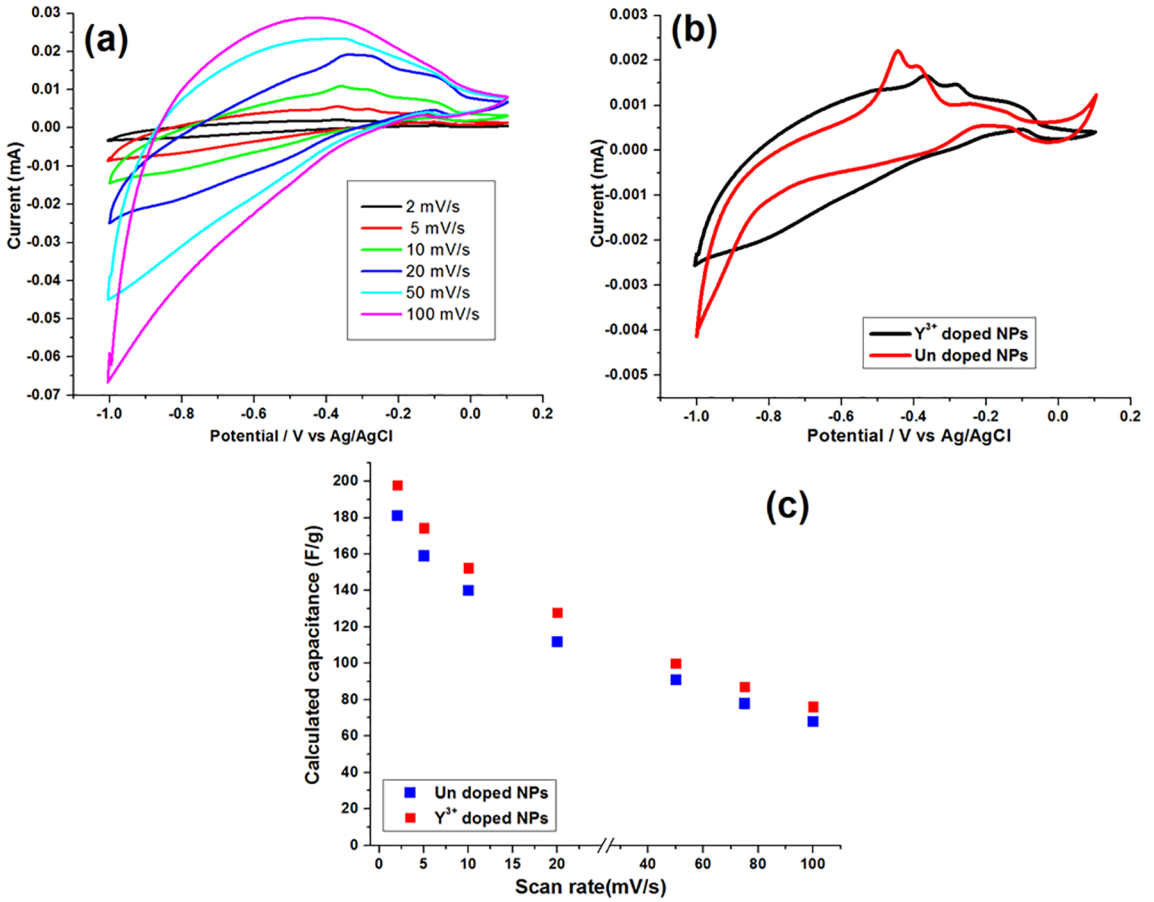

Fig. 5. (a) CVs of the fabricated Y-IONPs working electrode at the various scan rates, (b) (c) CV Yofiles for undped and Y3+doped MNPs at the scan rate of 5mV/s, and (c) the calculated specific capacitances for both electrodes vs. scan rate.

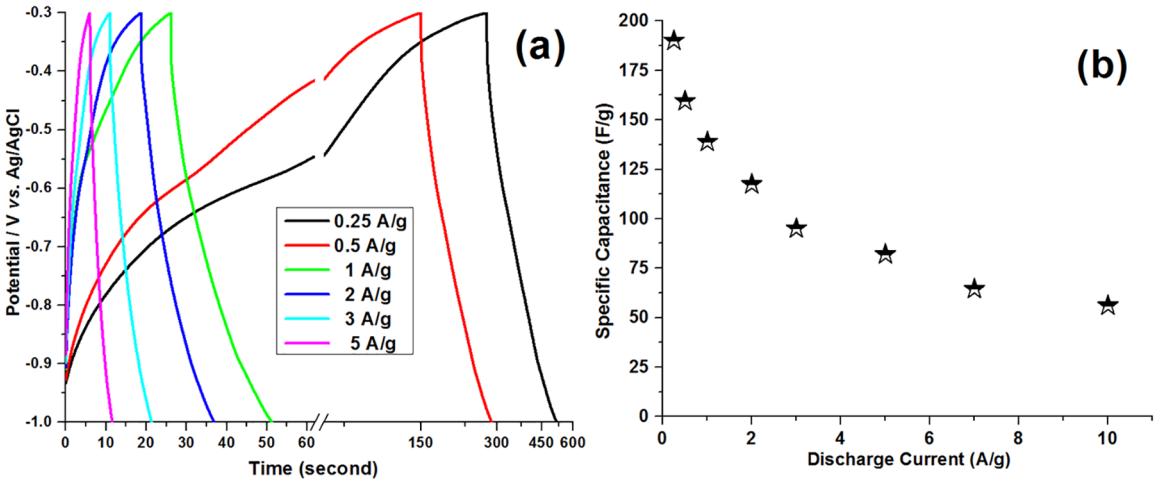

Fig. 6. (a) GCD Yofiles of Y-IONPs electrode and (b) is calculated SCs at the different current loads of 0.25 to 5 A g^{-1}

loads of 0.25, 0.5, 1, 2, 3, 5, 7 and 10 A g^{-1}, respectively. These values are close to those calculated based on the CVs (Fig. 5b), confirming the excellent super-capacitive behavior for the electro-synthesized Y^{3+} doped Fe_3O_4 nanoparticles. Furthermore, the charge storage ability of our prepared Y-IONPs sample is comparable with the reported SC data for the nanostructured Fe_3O_4 electrodes in the literature, which listed in Table 2.

Comparing the SC values listed in Table 2 revealed that the supercapacitive performance of our prepared Y-IONPs is higher than those reported for pure iron oxide electrodes, and hence the enhancement of charge storage ability of iron oxide through yttrium cations doping is confirmed.

The fabricated working electrode was further cycled (2000 cycles) at the current loads of 0.25 and 1 A g^{-1} in 1M Na_2SO_3 electrolyte. The SC values and capacity retentions of the fabricated Y-IONPs were calculated during cycling. Figs. 7a and b represent the SCs and SC retentions vs. cycle number, respectively. It was found that the SC value of Y^{3+} doped Fe_3O_4 NPs is reduced from 190.3 F g^{-1} to 182.5 F g^{-1} after 2000 GCD cycling at a discharging current of 0.25 A g^{-1} (Fig. 7a), which exhibited about 95.9% capacity retention, as seen in Fig. 7b. Also, the fabricated Y^{3+} doped NPs enable to deliver specific capacitance as high as 122.9 F g^{-1} after 2000 GCD cycles at a current of 1 A g^{-1}, which showed that the electrode had capacity retention of 88.5%

Table 2. Electrochemical capacitance values reported for Fe3O4 based working electrodes

Structure type	Electrolyte	Current density (A/g)	Specific capacitance (F/g)	Refs.
Nanocrystal	3M KOH	1 mA	185	[27]
Nanoparticles	1M Na_2SO_3	0.4	207.7	[30]
Octadecahedrons	1M Na_2SO_3	0.6	118.2	[36]
Thin film	1M Na_2SO_3	0.5	95	[37]
Spheroidal nanoassembles	1M Na_2SO4	0.5	48	[38]
Nanoparticles	6M KOH	1	160	[39]
Particle	3 M KOH	0.1	~120	[40]
Sub-micron spheres	8M KOH	0.5	294.5	[42]
Mn^{2+}doped Microspheres	1M KOH	1	268.4	[44]
Nanowires	0.1M Na_2SO_3	0.4	106	[46]
Nanoparticles	0.1M Na_2SO_3	0.4	12	[46]
Pyrrole treated nanowires	0.1M Na_2SO_3	0.4	190	[46]
Nanosheets	1M Na_2SO_3	0.42	83	[47]
Pristine nanospheres	1M Na_2SO_3	1	157.6	[48]
undoped Nanoparticles	1M Na_2SO_3	0.5	188	[51]
Y^{3+}doped Nanoparticles	1M Na_2SO_3	0.5	212.5	This work

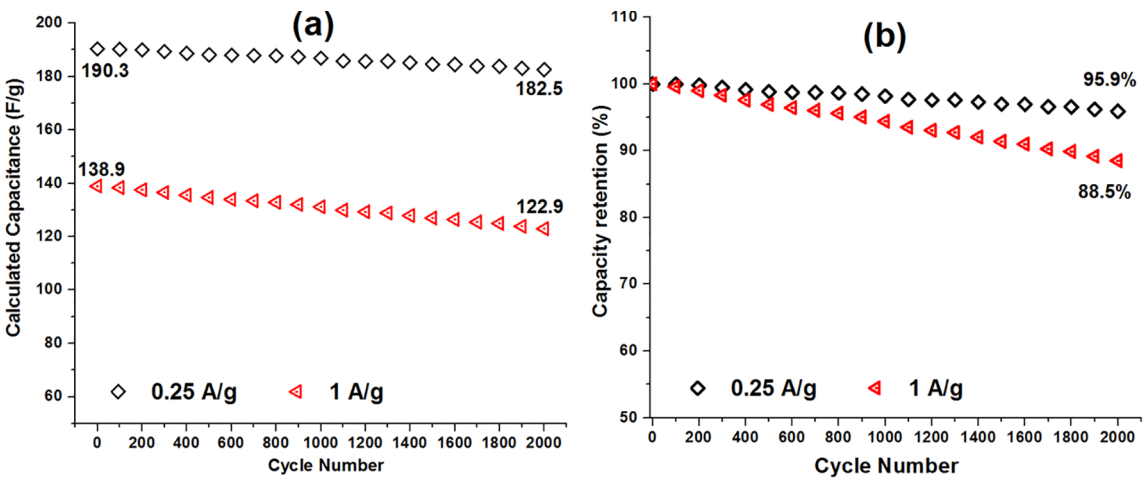

Fig. 7. (a) Calulated specific capacity valuess and (b) capacity retentions during 2000 GCD cycling at the discharge loads of 0.25 and 1 A g^{-1}

at this discharging rate (Fig. 7b). These data confirmed the proper charge storage ability of Y^{3+} doped Fe_3O_4 nanoparticles.

The energy and power densities of the fabricated working electrode were also calculated using Eqs.(7 and 8) [27]:

$$E = [C(\Delta V)^2]/2 \quad (7)$$

$$P = E/\Delta t \quad (8)$$

where E, C, ΔV, P and Δt are the specific energy, specific capacitance, potential window, specific power and discharge time, respectively. It was found that our electrode provides energy density and power density as high as 27.7 Wh/g and 8.02W/kg, respectively. These electrochemical data provides the proper supercapacitive performance of the electro-synthesized Y^{3+} doped Fe_3O_4nanoparticles.

4. Conclusion

In summary, a novel and easy electrochemical procedure was developed for the fabrication of Y^{3+} doped magnetite nanoparticles. The XRD, FE-SEM and EDS analyses proved the magnetite phase, fine particle morphology with 20 nm in size and 10%wt Y^{3+} content of the electrosynthesized iron oxide products. Galvanostat charge-discharging the fabricated electrode materials indicated that the Y^{3+} doped Fe_3O_4 nanoparticles are capable to deliver specific capacitances as high as with delivering a specific capacitance values of 190.3, 159.4, 138.9, 117.5, 96.7, 82, 66.8 and 55.9 F g^{-1} at the discharging loads of 0.25, 0.5, 1, 2, 3, 5, 7 and 10 A g^{-1}, respectively. It was found that the supercapacitive ability of magnetite nanoparticles is increased up to 20% thought Y^{3+} doping.

5. Conflict of interest

The authors declare that there is no conflict of interest about publishing this paper.

6. References

1. Wang Y, Song Y, Xia Y. Electrochemical capacitors: mechanism, materials, systems, characterization and applications. *Chemical Society Reviews*. 2016;45(21):5925-5950.

2. Xu CH, Chiu YF, Yeh PW, Chen JZ. SnO2/CNT nanocomposite supercapacitors fabricated using scanning atmospheric-pressure plasma jets. *Materials Research Express*. 2016;3(8):085002.

3. Aravinda LS, Nagaraja KK, Nagaraja HS, Udaya Bhat U, Ramachandra Bhat B. Fabrication and performance evaluation of hybrid supercapacitor electrodes based on carbon nanotubes and sputtered TiO2. *Nanotechnology*. 2016;27(31):314001.

4. Aghazadeh M, Ahmadi R, Gharailou D, Ganjali MR, Norouzi P. A facile route to preparation of Co3O4 nanoplates and investigation of their charge storage ability as electrode material for supercapacitors. *Journal of Materials Science: Materials in Electronics*. 2016;27(8):8623-8632.

5. Kim HJ, Kim SY, Lim LJ, Reddya AE, Muralee Gopi CVV. Facile one-step synthesis of a composite CuO/Co3O4 electrode material on Ni foam for flexible supercapacitor applications. *New Journal of Chemistry*. 2017;41(13):5493-5497.

6. Wang S, Li W, Xin L, Wu M, Sun W, Lou X. Pollen-inspired synthesis of porous and hollow NiO elliptical microstructures assembled from nanosheets for high-performance electrochemical energy storage. *Chemical Engineering Journal*. 2017;321:546-553.

7. Han Y, Zhang S, Shen N, Li D, Li X. MOF-derived porous NiO nanoparticle architecture for high performance supercapacitors. *Materials Letters*. 2017;188:1-4.

8. Liu Q, Lu C, Ying L. Controllable synthesis of ultrathin nickel oxide sheets on carbon cloth for high-performance supercapacitors. *RSC Advances*. 2017;7(37):23143-23148.

9. Do QH, Fielitz TR, Zeng C, Vanli OA, Zhang C, Zheng JP. Vanadium oxide-carbon nanotube composite electrodes for energy storage by supercritical fluid deposition: experiment design and device performance. *Nanotechnology*. 2013;24(31):315401.

10. He X, Yoo JE, Lee MH, Bae J. Morphology engineering of ZnO nanostructures for high performance supercapacitors: enhanced electrochemistry of ZnO nanocones compared to ZnO nanowires. *Nanotechnology*. 2017;28(24):245402.

11. Chen H, Wang MQ, Yu Y, Liu H, Lu SY, Bao SJ, et al. Assembling Hollow Cobalt Sulfide Nanocages Array on Graphene-Like Manganese Dioxide Nanosheets for Superior Electrochemical Capacitors. *ACS Applied Materials and Interfaces*. 2017;9(40):35040-35047.

12. Aghazadeh M, Maragheh MG, Ganjali MR, Norouzi P, Gharailou D, Faridbod F. Electrochemical preparation and supercapacitive performance of a-MnO2 nanospheres with secondary wall-like structures. *Journal of Materials Science: Materials in Electronics*. 2016:27(7):7707-7714.

13. de Oliveira AHP, Nascimento MLF, de Oliveira HP. Carbon nanotube@MnO2 @Polypyrrole Composites: Chemical Synthesis, Characterization and Application in Supercapacitors. *Materials Research*. 2016;19(5):1080-1087.

14. Jaggi N, Sharma D, Sharma P. MnO2/PVP/MWCNT hybrid nano composites as electrode materials for high performance supercapacitor. *Materials Research Express*. 2016;3(10):105503.

15. Liu Y, Wang N, Yao M, Yang C, Hu W, Komarneni S. Porous Ag-doped MnO2 thin films for supercapacitor electrodes. *Journal of Porous Materials*. 2017;24(6):1717-1723.

16. Zha D, Sun H, Fu Y, Ouyang X, Wang X. Acetate anion-intercalated nickel-cobalt layered double hydroxide nanosheets supported on Ni foam for high-performance supercapacitors with excellent long-term cycling stability. *Electrochimica Acta*. 2017;236:18-27.

17. Pang H, Li X, Zhao Q, Xue H, Lai WY, Hu Z, et al. One-pot synthesis of heterogeneous Co3O4-nanocube/Co(OH)2-nanosheet hybrids for high-performance flexible asymmetric all-solid-state supercapacitors. *Nano Energy*. 2017;35:138-145.

18. Ulaganathan M, Maharjan M, Yan Q, Aravindan V, Madhavi S. ß-Co(OH)2 Nanosheets: A Superior Pseudocapacitive Electrode for High-Energy Supercapacitors. *Chemistry - An Asian Journal*. 2017;12(16):2127-2133.

19. Aghazadeh M, Dalvand S, Hosseinifard M. Facile electrochemical synthesis of uniform ß-Co (OH)2 nanoplates for high performance supercapacitor. *Ceramics International*. 2014;40(2):3485-3493.

20. Yavuz A, Haciibrahimoglu MY, Bedir M. Synthesis and characterisation of Co-Co(OH)2 composite anode material on Cu current collector for energy storage devices. *Materials Research Express*. 2017;4(4):045502.

21. Zeng Z, Sun P, Zhu J, Zhu X. Porous petal-like Ni(OH)2-MnOx nanosheet electrodes grown on carbon fiber paper for supercapacitors. *Surfaces and Interfaces*. 2017;8:73-82.

22. Li W, Yang LL, Lin B, Isimjan TT, Yang DQ, Hu Y, et al. Large-scale synthesis of 3D sphere-like hierarchical Ni(OH)2 nanofibers for high-performance electrochemical supercapacitors. *Materials Research Express*. 2015;2(9):095008.

23. Dong B, Zhou H, Liang J, Zhang L, Gao G, Ding S. One-step synthesis of free-standing a-Ni(OH)2 nanosheets on reduced graphene oxide for high-performance supercapacitors. *Nanotechnology*. 2014;25(43):435403.

24. Ravi Kumar CR, Santosh MS, Nagaswarupa HP, Prashantha SC, Yallappa S, Anil Kumar MR. Synthesis and characterization of ß-Ni(OH)2 embedded with MgO and ZnO nanoparticles as nanohybrids for energy storage devices. *Materials Research Express*. 2017;4(6):065503.

25. Wu J, Ge F, Li Y. Preparation of Ni(OH)2/MWCNTs Composite for Supercapacitor Application. *International Journal of Electrochemical Science*. 2017;12:9665-9674.

26. Ke Q, Tang C, Liu Y, Liu H, Wang J. Intercalating graphene with clusters of Fe3O4 nanocrystals for electrochemical supercapacitors. *Materials Research Express*. 2014;1(2):025015.

27. Mitchell E, Gupt RK, Mensah-Darkwa K, Kumar D, Ramasamy K, Gupta BK, et al. Facile synthesis and morphogenesis of superparamagnetic iron oxide nanoparticles for high-performance supercapacitor applications. *New Journal of Chemistry*. 2014;38(9):4344-4350.

28. Aghazadeh M, Karimzadeh I, Ganjali MR. Electrochemical evaluation of the performance of cathodically grown ultra-fine magnetite nanoparticles as electrode material for supercapacitor applications. *Journal of Materials Science: Materials in Electronics*. 2017;28(18):13532-13539.

29. Li Z, Zhang Y, Zhang W. Controlled synthesis of CNTs/MoS2/Fe3O4 for high-performance supercapacitors. *Materials Research Express*. 2017;4(5):055018.

30. Wang L, Ji H, Wang S, Kong L, Jiang X, Yang G. Preparation of Fe3O4 with high specific surface area and improved capacitance as a supercapacitor. *Nanoscale*. 2013;5(9):3793-3799.

31. Kim M, Kim J. Synergistic interaction between pseudocapacitive Fe3O4 nanoparticles and highly porous silicon carbide for high-performance electrodes as electrochemical supercapacitors. *Nanotechnology*. 2017;28(19):195401.

32. Wu Q, Chen M, Chen K, Wang S, Wang C, Diao G. Fe3O4-based core/shell nanocomposites for high-performance electrochemical supercapacitors. *Journal of Materials Science*. 2016;51(3):1572-1580.

33. Nithya VD, Arul NS. Progress and development of Fe3O4 electrodes for supercapacitors. *Journal of Materials Chemistry A*. 2016;4(28):10767-10778.

34. Wang Y, He P, Zhao X, Lei W, Dong F. Coal tar residues-based nanostructured activated carbon/Fe3O4 composite electrode materials for supercapacitors. *Journal of Solid State Electrochemistry*. 2014;18(3):665-672.

35. Guo Z, Shin K, Karki AB, Young DP, Kaner RB, Hahn HT. Fabrication and characterization of iron oxide nanoparticles filled polypyrrole nanocomposites. *Journal of Nanoparticle Research*. 2009;11(6):1441-1452.

36. Chen J, Huang K, Liu S. Hydrothermal preparation of octadecahedron Fe3O4 thin film for use in an electrochemical supercapacitor. *Electrochimica Acta*. 2009;55(1):1-5.

37. Wang SY, Ho KC, Kuo SL, Wu NL. Investigation on Capacitance Mechanisms of Fe3O4 Electrochemical Capacitors. *Journal of The Electrochemical Society*. 2006;153(1):A75-A80.

38. Maqbool Q, Singh C, Paul A, Srivastava A. Uniform spheroidal nanoassemblies of magnetite using tween surfactants: influence of surfactant structure on the morphology and electrochemical performance. *Journal of Materials Chemistry: C*. 2015;3(7):1610-1618.

39. Liu S, Guo S, Sun S, You XZ. Dumbbell-like Au-Fe3O4 nanoparticles: a new nanostructure for supercapacitors. *Nanoscale*. 2015;7(11):4890-4893.

40. Hallam PM, Gómez-Mingot M, Kampouris DK, Banks CE. Facile synthetic fabrication of iron oxide particles and novel hydrogen superoxide supercapacitors. *RSC Advances*. 2012;2(16):6672-6679.

41. Ganganboina AB, Chowdhury AD, Doong R. Nano assembly of N-doped graphene quantum dots anchored Fe3O4/halloysite nanotubes for high performance supercapacitor. *Electrochimica Acta*. 2017;245:912-923.

42. Zeng X, Yang B, Li X, Li R, Yu R. Solvothermal synthesis of hollow Fe3O4 sub-micron spheres and their enhanced electrochemical properties for supercapacitors. *Materials & Design*. 2016;101:35-43.

43. Li L, Gao P, Gai S, He F, Chen Y, Zhang M, et al. Ultra-small and highly dispersed Fe3O4 nanoparticles anchored on reduced graphene for supercapacitor application. *Electrochimica Acta*. 2016;190:566-573.

44. Yang X, Kan J, Zhang F, Zhu M, Li S. Facile Fabrication of Mn2+ Doped Magnetite Microspheres as Efficient Electrode Material for Supercapacitors. *Journal of Inorganic and Organometallic Polymers and Materials*. 2017;27(2):542-551.

45. Mezgebe MM, Yan Z, Wei G, Gong S, Zhang F, Guang S, et al. 3D graphene-Fe3O4-polyaniline, a novel ternary composite for supercapacitor electrodes with improved electrochemical properties. *Materials Today Energy*. 2017;5:164-172.

46. Zhao X, Johnston C, Crossley A, Grant PS. Printable magnetite and pyrrole treated magnetite based electrodes for supercapacitors. *Journal of Materials Chemistry*. 2010;20(36):7637-7644.

47. Mu J, Chen B, Guo Z, Zhang M, Zhang Z, Zhang P, et al. Highly dispersed Fe3O4 nanosheets on one-dimensional carbon nanofibers: Synthesis, formation mechanism, and electrochemical performance as supercapacitor electrode materials. *Nanoscale*. 2011;3(12):5034-5040.

48. Aghazadeh M, Ganjali MR, Norouzi P. Preparation of Mn5O8 and Mn3O4 nano-rods through cathodic electrochemical deposition-heat treatment (CED-HT). *Materials Research Express*. 2016;3(5):055013.

49. Aghazadeh M, Hosseinifard M. Electrochemical preparation of ZrO2 nanopowder: Impact of the pulse current on the crystal structure, composition and morphology. *Ceramics International*. 2012;39(4):4427-4435.

50. Karimzadeh I, Aghazadeh M, Ganjali MR, Norouzi P, Doroudi T, Kolivand PH. Saccharide-coated superparamagnetic Fe3O4 nanoparticles (SPIONs) for biomedical applications: An efficient and scalable route for preparation and in situ surface coating through cathodic electrochemical deposition (CED). *Materials Letters*. 2017;189:290-294.

51. Aghazadeh M, Ganjali MR. One-pot electrochemical synthesis and assessment of super-capacitive and super-paramagnetic performances of Co2+ doped Fe3O4 ultra-fine particles. *Journal of Materials Science: Materials in Electronics*. 2018;29(3):2291-2300.

52. Aghazadeh M, Ganjali MR. Samarium-doped Fe3O4 nanoparticles with improved magnetic and supercapacitive performance: a novel preparation strategy and characterization. *Journal of Materials Science*. 2018;53(1):295-308.

53. Aghazadeh M, Ganjali MR. Evaluation of supercapacitive and magnetic properties of Fe3O4 nano-particles electrochemically doped with dysprosium cations: Development of novel iron-based electrode. *Ceramics International*. 2018:44(1):520-529.

54. De Silva CR, Smith S, Shim I, Pyun J, Gutu T, Jiao J, et al. Lanthanide(III)-doped magnetite nanoparticles. *Journal of the American Chemical Society*. 2009;131(18):6336-6337.

55. Park JC, Yeo S, Kim M, Lee GT, Seo JH. Synthesis and characterization of novel lanthanide-doped magnetite@Au core@shell nanoparticles. *Materials Letters*. 2016;181:272-277.

56. Douglas FJ, MacLaren DA, Maclean N, Andreu I, Kettles FJ, Tuna F, et al. Gadolinium-doped magnetite nanoparticles from a single-source precursor. *RSC Advances*. 2016;6(78):74500-74505.

57. Thi TM, Huyen Trang NT, Van Anh NT. Effects of Mn, Cu doping concentration to the properties of magnetic nanoparticles and arsenic adsorption capacity in wastewater. *Applied Surface Science*. 2015;340:166-172.